

PAPER • OPEN ACCESS

Ni self-diffusion in glass forming Pd–Ni–S melts

To cite this article: Johanna Wilden *et al* 2021 *J. Phys.: Condens. Matter* **33** 435101

View the [article online](#) for updates and enhancements.

You may also like

- [Core-Shell Pd₉Ru@Pt on Functionalized Graphene for Methanol Electrooxidation](#)
Chih-Chia Kuo, Shih-Cheng Chou, Yu-Chen Chang *et al.*
- [The adsorption of small size Pd clusters on a g-C₃N₄ quantum dot: DFT and TD-DFT study](#)
Sayyed Mahdi Hosseini, Mehran Ghiaci and Hossein Farrokhpour
- [Enhancement of Electrocatalytic Oxygen Reduction Reaction on Pd₉Pb Ordered Intermetallic Catalyst in Alkaline Aqueous Solutions](#)
Futoshi Matsumoto, Arockiam John Jeevagan, Takao Gunji *et al.*



IOP | ebooks™

Bringing together innovative digital publishing with leading authors from the global scientific community.

Start exploring the collection—download the first chapter of every title for free.

Ni self-diffusion in glass forming Pd–Ni–S melts

Johanna Wilden^{1,*}, Fan Yang¹, Gerrit Günther², Margarita Russina²,
Alexander Kuball^{3,4}, Ralf Busch³ and Andreas Meyer¹

¹ Institut für Materialphysik im Weltraum, Deutsches Zentrum für Luft- und Raumfahrt (DLR), 51170 Köln, Germany

² Helmholtz-Zentrum Berlin für Materialien und Energie, 14109 Berlin, Germany

³ Lehrstuhl für metallische Werkstoffe, Universität des Saarlandes, 66123 Saarbrücken, Germany

⁴ Amorphous Metal Solutions GmbH, 66424 Homburg, Germany

E-mail: johanna.wilden@dlr.de

Received 17 May 2021, revised 16 July 2021

Accepted for publication 30 July 2021

Published 18 August 2021



Abstract

The Ni self-diffusion in glass forming Pd₄₀Ni₄₀S₂₀, Pd₃₇Ni₃₇S₂₆ and Pd₃₁Ni₄₂S₂₇ melts was probed by incoherent, quasielastic neutron scattering over a temperature range between 773 and 1023 K. The Ni self-diffusion coefficients are on a 10⁻¹⁰ m² s⁻¹–10⁻⁹ m² s⁻¹ scale and barely change with composition. Each composition exhibits an Arrhenius-type temperature dependence of the Ni self-diffusion coefficients, which results in activation energies ranging from $E_A = 348 \pm 16$ meV for Pd₄₀Ni₄₀S₂₀ to $E_A = 387 \pm 6$ meV for Pd₃₇Ni₃₇S₂₆. The structural relaxation shows a stretched exponential behavior even far above the liquidus temperatures. In addition, the viscosity of the Pd₃₇Ni₃₇S₂₆ melt was measured under reduced gravity conditions. The diffusion calculated from the viscosity reveals a significant deviation from the measured Ni self-diffusion by a factor between 4 and 8. This may indicate a dynamic decoupling between the atoms within the Pd–Ni–S equilibrium melts.

Keywords: self-diffusion, viscosity, metallic melts, bulk metallic glasses, sulfur, quasielastic neutron scattering

(Some figures may appear in colour only in the online journal)

1. Introduction

Ni–P-based alloys are very well explored bulk metallic glass formers. Within the ternary Pd–Ni–P system, Pd₄₀Ni₄₀P₂₀ represents the best glass former [1–4] and thus enables the casting of glassy cylinders with 25 mm in diameter by fluxing in dehydrated B₂O₃ and subsequent water quenching [4]. As a result of its excellent glass forming ability, Pd–Ni–P became a model system to study bulk metallic glass formation [5–7]. In order to understand the glass formation in Ni–P-based alloys, the melt dynamics were examined. The viscosity

describes the flow behavior and therefore the melt dynamics on a macroscopic scale, whereas the self-diffusion describes the atomic motion and therefore the melt dynamics on a microscopic scale. Within Ni, Ni–P, Pd–Ni–P and Pd–Ni–Cu–P melts, a previous study shows that the Ni/(Cu) self-diffusion barely changes with composition [8]. The same holds for the packing fraction. Thus, the authors came to the conclusion that the atomic motion is determined by the packing fraction [8, 9]. This implies that these melts behave like monatomic metallic melts above the critical temperature of mode coupling theory [10]. In this case, the atoms can be approximated as hard spheres with defined radii [11]. Thus, the atomic bonds are non-directional and neglect all kind of chemical interactions. Since the melt dynamics in Ni, Ni–P, Pd–Ni–P and Pd–Ni–Cu–P barely change with composition, the enhanced glass forming ability reveals no dynamic origin. It is rather

* Author to whom any correspondence should be addressed.

Original content from this work may be used under the terms of the [Creative Commons Attribution 4.0 licence](https://creativecommons.org/licenses/by/4.0/). Any further distribution of this work must maintain attribution to the author(s) and the title of the work, journal citation and DOI.

related to thermodynamics, since the liquidus temperature decreases with the number of elements [8].

It was recently found that the replacement of P by S leads to bulk metallic glass formation as well [12, 13]. Within the ternary Pd–Ni–S system, Pd₃₇Ni₃₇S₂₆ represents the best glass former with a critical casting thickness of 2 mm, whereas Pd₃₁Ni₄₂S₂₇ exhibits the best thermal stability against crystallization upon heating from the glassy state [12, 13]. A recent study on Ti–Ni–S melts reveals that S-addition affects the melt dynamics differently [14] than element addition in Ni–P-based melts [8]. Here the Ti/Ni self-diffusion and the packing fraction decrease simultaneously upon S-addition. For this reason, the reduced melt dynamics cannot be explained by a dense packing of hard spheres. The decrease of the packing fraction upon S-addition indicates the occurrence of directional bonds, which may develop a pronounced chemical short-range-order. This could be the origin for the improved glass formation in Ti–Ni–S.

Besides the reduced packing fraction, the decoupling of the self-diffusion coefficients indicates the occurrence of a chemical short-range order. In Zr-based melts the self-diffusion of the large Zr atoms and the smaller atoms diverges above the liquidus temperature [15, 16]. The authors argue that the decoupling is caused by a Zr-network, which contains strong directional bonds [15]. In contrast, all atoms within the Pd–Ni–(Cu)–P equilibrium melts exhibit similar self-diffusion coefficients [17]. The decoupling in Pd–Ni–(Cu)–P only occurs below the critical temperature of the mode-coupling-theory [18]. Here the self-diffusion of the large Pd atoms and the smaller Ni, Cu and P atoms start to diverge [18, 19].

In this study, we examined how S affects the melt dynamics in Pd–Ni–S and compared our results to the melt dynamics in Ni–P-based systems and Ti–Ni–S. Therefore, we probed the Ni self-diffusion and its temperature dependence by incoherent, quasielastic neutron scattering [20]. This method is not affected by fluid flow, since it measures on atomic time- and length-scales. Thus, accurate Ni self-diffusion coefficients can be obtained on an absolute scale. In order to estimate whether a dynamic decoupling occurs in Pd–Ni–S melts above the liquidus temperature like in Zr-based melts, the viscosity of Pd₃₇Ni₃₇S₂₆ was measured under reduced gravity conditions by electromagnetic levitation. Furthermore, the sample volume was determined from the reduced gravity data, which enabled the calculation of the packing fraction. With this, the correlation between self-diffusion and packing fraction in Pd₃₇Ni₃₇S₂₆ melts was crosschecked.

2. Experimental

To produce the Pd–Ni–S master alloys the raw elements Pd (99.999 wt.%), Ni (99.95 wt.%) and S (99.9995 wt.%) were inductively melted in silica tubes under a high purity Ar-atmosphere [13]. Subsequently, the alloys were remelted and fluxed in dehydrated B₂O₃ in order to remove oxide impurities [13]. To prepare the samples for the quasielastic neutron scattering experiments in Al₂O₃ containers, they were suction cast into Cu-molds with 4 mm in diameter.

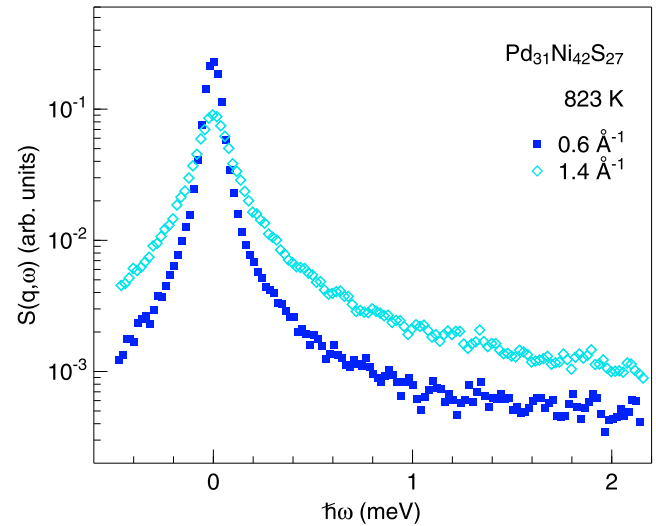


Figure 1. Scattering law $S(q, \omega)$ of liquid Pd₃₁Ni₄₂S₂₇ for $q = 0.6 \text{ \AA}^{-1}$ and $q = 1.4 \text{ \AA}^{-1}$ at 823 K.

The liquid samples were measured in 0.5 mm thick Al₂O₃ containers with 5 mm in diameter and 40 mm in height at the neutron time-of-flight spectrometer NEAT [21, 22] located at the BER-2 neutron source (Helmholtz-Zentrum Berlin, Germany). The setup with a neutron wavelength of $\lambda = 6 \text{ \AA}$ gives an accessible wavenumber range of $q = 0.5$ to 1.7 \AA^{-1} at zero energy transfer and an instrumental energy resolution of $63 \mu\text{eV}$ at full width half maximum. During the experiments the samples were annealed under vacuum in a Nb electrical resistance furnace that provides a temperature stability of better than $\pm 0.5 \text{ K}$. The time-of-flight spectra were taken above the liquidus temperatures (T_L (Pd₄₀Ni₄₀S₂₀): 744.0 K, T_L (Pd₃₇Ni₃₇S₂₆): 730.8 K, T_L (Pd₃₁Ni₄₂S₂₇): 756.0 K [13]) between 773 and 973 K in steps of 50 K and with an exposure time of 120 min at each temperature. For Pd₃₇Ni₃₇S₂₆ an additional measurement was performed at 1023 K. The samples mass loss after the experiments was well below 0.1%. A measurement of the samples at room temperature served as the instrumental energy resolution of the time-of-flight spectrometer. In order to obtain the scattering law $S(q, \omega)$, the measured time-of-flight spectra $I(2\theta, \text{tof})$ were normalized to a vanadium standard, interpolated to constant wavenumbers and corrected for empty container scattering. For precise description of the evaluation procedure, the reader is referred to [20]. Figure 1 shows the scattering law $S(q, \omega)$ of liquid Pd₃₁Ni₄₂S₂₇ for $q = 0.6 \text{ \AA}^{-1}$ and $q = 1.4 \text{ \AA}^{-1}$ at 823 K. At small wavenumbers the scattering signal is governed by the incoherent scattering cross section of Ni ($\sigma_{\text{inc.}}(\text{Ni}) = 5.2(4) \text{ barn}$ [23]), whereas the incoherent cross sections of Pd ($\sigma_{\text{inc.}}(\text{Pd}) = 0.093(9) \text{ barn}$ [23]) and S ($\sigma_{\text{inc.}}(\text{S}) = 0.007(5) \text{ barn}$ [23]) can be neglected. Within the examined q -range two coherent contributions need to be considered [20]: (1) the coherent part that results from thermal diffusion, which appears as a Rayleigh line within the scattering law $S(q, \omega)$. Since the thermal diffusion is much faster than the self-diffusion in metals, the Rayleigh line appears as a flat background within the examined energy range. (2) The coherent part that results from phonons, which appears

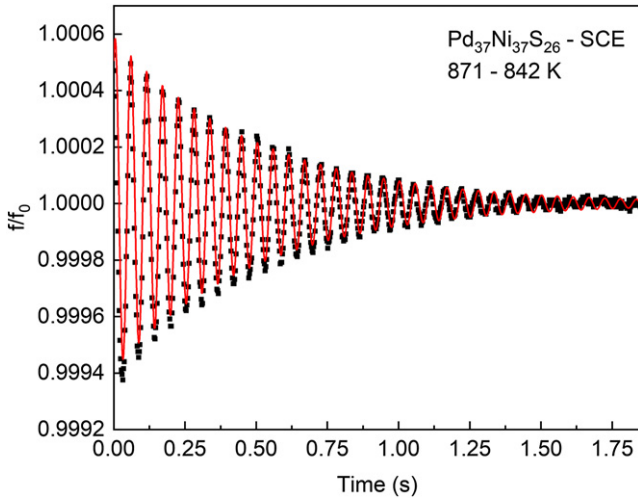


Figure 2. Normalized coupling frequency f/f_0 as a function of time t for the oscillation decay in liquid $\text{Pd}_{37}\text{Ni}_{37}\text{S}_{26}$ during cooling between 871 and 842 K. This data set was recorded by the SCE during a parabolic flight with TEMPUS. The red, solid line represents a fit with $f(t) = f_0 + A \exp(-t/\tau) \sin(\omega t + \delta_0)$, where f_0 is the initial coupling frequency, A is the oscillation amplitude, τ is the decay constant, ω is the circular frequency and δ_0 is the phase shift.

as two Brillouin lines within the scattering law $S(q, \omega)$. However, these Brillouin lines are located outside the examined energy range. Thus, the coherent contribution can be neglected compared to incoherent contribution of Ni. Fourier deconvolution of the scattering law $S(q, \omega)$ and normalization to 1 for $t = 0$ gives the intermediate scattering function $S_0(q, t)$.

The viscosity of liquid $\text{Pd}_{37}\text{Ni}_{37}\text{S}_{26}$ was measured within reduced gravity cycles of about 22 s. This was realized by container-less processing during parabolic flights with the TEMPUS facility [24]. In contrast to ground-based electromagnetic levitation, magnetic fields in TEMPUS are small enough to permit viscosity measurements by the oscillation drop technique [25–27]. Here the surface oscillation decay of liquid $\text{Pd}_{37}\text{Ni}_{37}\text{S}_{26}$ was recorded during cooling. The decay constant provides information on the viscosity ($\eta = \rho R_0^2 / 5\tau$ [28], where ρ is the melt density, R_0 is the initial radius and τ is the decay constant) over a certain temperature range, as shown in figure 2. The decay curves were recorded by a newly installed infrared (IR) camera (frame rate: 1000 fps), which enables the detection of melts with low liquidus temperatures. At the same time, the decay curves were recorded by sample coupling electronics (SCE) (frame rate: 400 fps), which additionally provide information on the sample volume [29]. In order to obtain absolute values for the sample volume, a calibration with a Zr sphere was performed.

3. Results and discussion

The intermediate scattering functions $S_0(q, t)$ were fitted by the Kohlrausch–Williams–Watts stretched exponential function within the α relaxation regime:

$$S_0(q, t) = A \exp[-(t/\tau)^\beta], \quad (1)$$

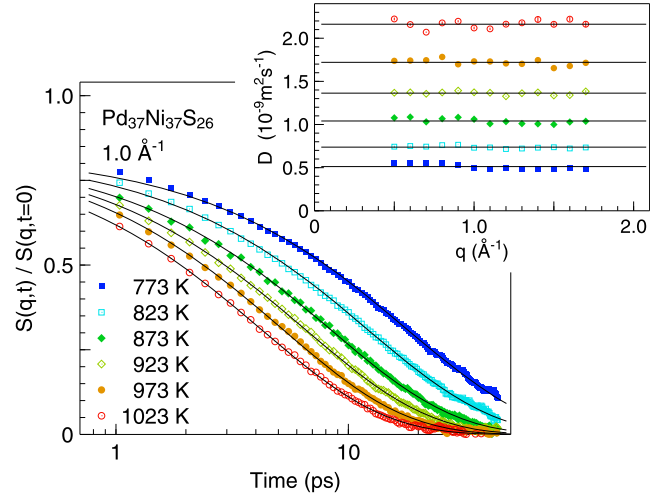


Figure 3. Intermediate scattering function $S_0(q, t)$ of liquid $\text{Pd}_{37}\text{Ni}_{37}\text{S}_{26}$ for $q = 1 \text{ \AA}^{-1}$ at different temperatures between 773 and 1023 K. The solid lines are fits with the Kohlrausch–Williams–Watts stretched exponential function (equation (1)). The insert shows the self-diffusion coefficients calculated from the relaxation times as a function of the wavenumber.

where A is the structural relaxation amplitude, τ is the structural relaxation time, and β is the stretching exponent. The onset of glassy dynamics results in a deviation from an exponential decay ($\beta < 1.0$) [30–32]. The best fit results in a q - and temperature-independent stretching exponent $\beta = 0.82$. Figure 3 shows the intermediate scattering function $S_0(q, t)$ of liquid $\text{Pd}_{37}\text{Ni}_{37}\text{S}_{26}$ for $q = 1 \text{ \AA}^{-1}$ at six different temperatures. The solid lines correspond to fits with the Kohlrausch–Williams–Watts stretched exponential function (equation (1)). The inset in figure 3 shows the self-diffusion coefficients ($D = 1/(\tau q^2)$) calculated from the relaxation times as a function of the wavenumber [33]. For all temperatures the self-diffusion coefficients are constant over the entire q -range, which confirms the diffusive nature of the melt dynamics. Since the incoherent scattering cross section of Pd–Ni–S melts is dominated by Ni, D represents the Ni self-diffusion coefficient.

Figure 4 shows the Ni self-diffusion coefficients of the $\text{Pd}_{40}\text{Ni}_{40}\text{S}_{20}$, $\text{Pd}_{37}\text{Ni}_{37}\text{S}_{26}$ and $\text{Pd}_{31}\text{Ni}_{42}\text{S}_{27}$ melts probed by incoherent, quasielastic neutron scattering as function of inverse temperature. The Ni self-diffusion coefficients range from $(5.0 \pm 0.2) \times 10^{-10} \text{ m}^2 \text{ s}^{-1}$ for $\text{Pd}_{40}\text{Ni}_{40}\text{S}_{20}$ at 773 K to $(2.16 \pm 0.12) \times 10^{-9} \text{ m}^2 \text{ s}^{-1}$ for $\text{Pd}_{37}\text{Ni}_{37}\text{S}_{26}$ at 1023 K and barely change with composition. In contrast, the Ti/Ni self-diffusion coefficients in Ti–Ni–S are much more sensitive to the S-content [14]. For comparison, the Ni self-diffusion coefficients of $\text{Pd}_{40}\text{Ni}_{40}\text{P}_{20}$ [8] and the Ni/Cu self-diffusion coefficients of $\text{Pd}_{40}\text{Ni}_{10}\text{Cu}_{30}\text{P}_{20}$ [34] are shown in figure 4. Here it becomes clear that the Ni/(Cu) self-diffusion in the melts with P is one order of magnitude slower. The temperature dependence of the Ni self-diffusion is similar for all Pd–Ni–S melts and can be described by an Arrhenius-type temperature dependence:

$$D(T) = D_0 \exp(-E_A/k_B T), \quad (2)$$

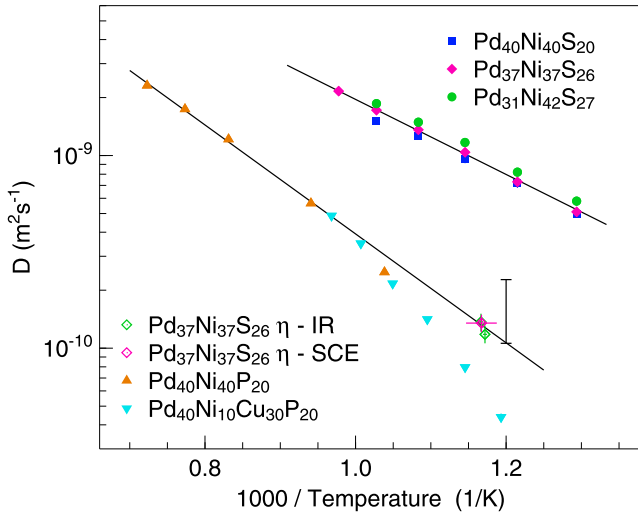


Figure 4. Ni/(Cu) self-diffusion coefficients in Pd₄₀Ni₄₀S₂₀, Pd₃₇Ni₃₇S₂₆, Pd₃₁Ni₄₂S₂₇, Pd₄₀Ni₄₀P₂₀ [8] and Pd₄₀Ni₁₀Cu₃₀P₂₀ [34] melts probed by quasielastic neutron scattering. The black lines are Arrhenius fits (equation (2)) for Pd₃₇Ni₃₇S₂₆ and Pd₄₀Ni₄₀P₂₀ [8]. In addition, the diffusion coefficients calculated from the measured viscosities (IR camera and SCE) in Pd₃₇Ni₃₇S₂₆ are shown. The error bar indicates the range in which the diffusion coefficients calculated by the Stokes–Einstein and the Sutherland–Einstein relation can scatter.

Table 1. Parameters obtained from Arrhenius fits of the Ni self-diffusion in Pd₄₀Ni₄₀S₂₀, Pd₃₇Ni₃₇S₂₆, Pd₃₁Ni₄₂S₂₇ and Pd₄₀Ni₄₀P₂₀ [8] melts.

Composition	D_0 ($10^{-7} \text{ m}^2 \text{ s}^{-1}$)	E_A (meV)
Pd ₄₀ Ni ₄₀ S ₂₀	0.98 ± 0.20	348 ± 16
Pd ₃₇ Ni ₃₇ S ₂₆	1.74 ± 0.12	387 ± 6
Pd ₃₁ Ni ₄₂ S ₂₇	1.31 ± 0.61	355 ± 37
Pd ₄₀ Ni ₄₀ P ₂₀	2.39 ± 0.56	551 ± 27

with the prefactor D_0 , the activation energy E_A and the Boltzmann constant $k_B = 8.617 \times 10^{-2} \text{ meV K}^{-1}$. The Arrhenius fit parameters are presented in table 1. In order to compare the activation energies for self-diffusion to Pd₄₀Ni₄₀P₂₀ [8], the quasielastic neutron scattering data was fitted by equation (2) and the Arrhenius fit parameters are also presented in table 1. The activation energy for self-diffusion in Pd₄₀Ni₄₀S₂₀ corresponds to $348 \pm 16 \text{ meV}$ and is thus 203 meV smaller than the one for Pd₄₀Ni₄₀P₂₀. This reflects the more fragile nature of Pd–Ni–S ($D^*(\text{Pd}_{31}\text{Ni}_{42}\text{S}_{27}) = 8.31$ [35]) compared to Pd–Ni–P ($D^*(\text{Pd}_{40}\text{Ni}_{40}\text{P}_{20}) = 18.1$ [36]). The activation energy in Pd–Ni–S melts corresponds to about the half of the activation energy in Ti₇₅Ni₂₀S₅ melts with $E_A = 657 \text{ meV}$ [14].

The sample coupling electronics data set from the reduced gravity experiments provides information on the sample volume. Together with the sample mass, the melt density was calculated. This enabled the determination of the packing fraction φ according to $\varphi = 4\pi/3 \times ((0.37r_{\text{Pd}})^3 + (0.37r_{\text{Ni}})^3 + (0.26r_{\text{S}})^3) \times \rho N_A / \bar{M}$, where $r_{\text{Pd}} = 1.28 \text{ \AA}$, $r_{\text{Ni}} = 1.15 \text{ \AA}$ and $r_{\text{S}} = 1.04 \text{ \AA}$ [37] are the covalent atomic radii, ρ is the melt density, N_A the Avogadro constant and \bar{M} is the average molar

mass. For the measured temperature interval an average packing fraction of 0.52 at 859 K was determined. This packing fraction was compared to the one of Pd₄₀Ni₄₀P₂₀ at the same temperature, which corresponds to 0.54. The increase in packing fraction upon S replacement by P correlates with the previous observed decrease in melt dynamics. Although S has a smaller atomic radius than P, it decreases the packing fraction and thus indicates the occurrence of a pronounced chemical short-range order.

We determined the viscosity of liquid Pd₃₇Ni₃₇S₂₆ during one parabola. Thus, we obtained a viscosity of $40 \pm 4 \text{ mPa s}$ between 859 and 856 K and a viscosity of $46 \pm 5 \text{ mPa s}$ between 855 and 852 K from the IR camera data set. From the sample coupling electronics data set we obtained a viscosity of $40 \pm 3 \text{ mPa s}$ between 871 and 842 K. In order to compare our data to literature values [30], we calculated the diffusion from the viscosity according to the Stokes–Einstein relation [38]:

$$D = k_B T / (6\pi r \eta), \quad (3)$$

where k_B is the Boltzmann constant, T is the average temperature and r the covalent radius of Ni = 1.15 Å [37]. The calculated diffusion coefficients correspond to $(1.37 \pm 0.15) \times 10^{-10} \text{ m}^2 \text{ s}^{-1}$ at $857 \pm 2 \text{ K}$ (IR camera), $(1.18 \pm 0.13) \times 10^{-10} \text{ m}^2 \text{ s}^{-1}$ at $853 \pm 2 \text{ K}$ (IR camera) and to $(1.35 \pm 0.14) \times 10^{-10} \text{ m}^2 \text{ s}^{-1}$ at $857 \pm 15 \text{ K}$ (sample coupling electronics), as presented in figure 4. According to the Arrhenius-type temperature dependence the measured Ni self-diffusion coefficients correspond to $8.99 \times 10^{-10} \text{ m}^2 \text{ s}^{-1}$ at 853 K and to $9.22 \times 10^{-10} \text{ m}^2 \text{ s}^{-1}$ at 857 K. Thus, the measured Ni self-diffusion coefficients are underestimated by a factor between 7 and 8. In Pd–Ni–Cu–P the deviation from the Stokes–Einstein relation does not exceed the factor of 2 within the equilibrium melt [18, 30].

Even under the consideration of the Sutherland–Einstein relation (4π instead of 6π) [39], as well as under the consideration of the covalent radius of Pd = 1.28 Å [37] the measured diffusion coefficient is underestimated by a factor between 4 and 8 (figure 4). This deviation suggests that the diffusion calculated from the viscosity is rather governed by the Pd or the S self-diffusion. In contrast to Ni–P-based alloys, the dynamic decoupling in Pd–Ni–S seems to initiate above the liquidus temperature. However, it is not so pronounced as the dynamic decoupling in Zr-based melts. In order to understand the dynamic decoupling in Pd–Ni–S above the liquidus temperature, shear cell experiments in microgravity are planned to determine the self-diffusion of ¹⁰⁸Pd, ⁶²Ni and ³⁴S.

4. Conclusion

In conclusion, we determined the Ni self-diffusion in Pd₄₀Ni₄₀S₂₀, Pd₃₇Ni₃₇S₂₆ and Pd₃₁Ni₄₂S₂₇ equilibrium melts by incoherent, quasielastic neutron scattering. The Ni self-diffusion coefficients were derived from the structural relaxation times and correspond to $3.75\text{--}5.60 \times 10^{-10} \text{ m}^2 \text{ s}^{-1}$ at the liquidus temperature, which is about one order of magnitude slower than for monatomic metallic melts (e.g. Ni [8]).

Furthermore, the structural relaxation is stretched exponential and best described by a q - and temperature-independent stretching exponent $\beta = 0.82$. The Ni self-diffusion barely changes with composition, as well as the Arrhenius-type temperature dependence. Thus, the activation energies vary only between 348 ± 16 and 387 ± 6 meV. Compared to Ni–P-based melts, Pd–Ni–S melts reveal faster melt dynamics, which is in accordance with the lower packing fraction. Furthermore, the viscosity in the Pd₃₇Ni₃₇S₂₆ equilibrium melt was probed within reduced gravity cycles. The diffusion calculated from the viscosity reveals a deviation from the diffusion measured in neutron scattering experiments by a factor between 4 and 8. This indicates a dynamic decoupling above the liquids temperature. Further shear cell experiments in microgravity are demanded to determine the individual Pd, Ni, S self-diffusion coefficients and thus the origin of dynamic decoupling.

Acknowledgments

We thank Elke Sondermann and Melanie Clozel for a critical reading of the manuscript. Another thank goes to Georg Lohöfer, who determined melt density of Pd₃₇Ni₃₇S₂₆ from the sample coupling electronics data set. Financial support by the Deutsche Forschungsgemeinschaft (DFG) through the Grants No. ME 1958/12-1 and BU 2276/11-1 is gratefully acknowledged.

Data availability statement

The data that support the findings of this study are available upon reasonable request from the authors.

Appendix.

See table A1.

Table A1. Ni self-diffusion in Pd₄₀Ni₄₀S₂₀, Pd₃₇Ni₃₇S₂₆ and Pd₃₁Ni₄₂S₂₇ melts probed by incoherent, quasielastic neutron scattering.

Composition	T (K)	D (10^{-9} m ² s ⁻¹)
Pd ₄₀ Ni ₄₀ S ₂₀	773 ± 0.5	0.50 ± 0.02
	823 ± 0.5	0.72 ± 0.04
	873 ± 0.5	0.96 ± 0.05
	923 ± 0.5	1.27 ± 0.06
	973 ± 0.5	1.51 ± 0.06
Pd ₃₇ Ni ₃₇ S ₂₆	773 ± 0.5	0.51 ± 0.03
	823 ± 0.5	0.73 ± 0.02
	873 ± 0.5	1.04 ± 0.03
	923 ± 0.5	1.36 ± 0.04
	973 ± 0.5	1.72 ± 0.05
	1023 ± 0.5	2.16 ± 0.12
Pd ₃₁ Ni ₄₂ S ₂₇	773 ± 0.5	0.58 ± 0.03
	823 ± 0.5	0.82 ± 0.02
	873 ± 0.5	1.30 ± 0.04
	923 ± 0.5	1.49 ± 0.04
	973 ± 0.5	1.86 ± 0.04

ORCID iDs

Johanna Wilden  <https://orcid.org/0000-0002-0434-2855>
 Fan Yang  <https://orcid.org/0000-0001-5281-2957>
 Gerrit Günther  <https://orcid.org/0000-0001-6243-1728>
 Alexander Kuball  <https://orcid.org/0000-0002-0053-1181>
 Andreas Meyer  <https://orcid.org/0000-0002-0604-5467>

References

- [1] Drehman A J, Greer A L and Turnbull D 1982 *Appl. Phys. Lett.* **41** 716–7
- [2] Kui H W, Greer A L and Turnbull D 1984 *Appl. Phys. Lett.* **45** 615–6
- [3] He Y, Schwarz R B and Archuleta J I 1996 *Appl. Phys. Lett.* **69** 1861–3
- [4] Schwarz R and He Y 1997 Formation and properties of bulk amorphous Pd–Ni–P alloys *Mater. Sci. Forum* **235** 231–40
- [5] Wilde G, Görler G P, Willnecker R and Dietz G 1994 *Appl. Phys. Lett.* **65** 397–9
- [6] Wilde G, Klose S G, Soellner W, Görler G P, Jeropoulos K, Willnecker R and Fecht H J 1997 *Mater. Sci. Eng. A* **226–228** 434–8
- [7] Lu I-R, Wilde G, Görler G P and Willnecker R 1999 *J. Non-Cryst. Solids* **250–252** 577–81
- [8] Chathoth S M, Meyer A, Koza M M and Juranyi F 2004 *Appl. Phys. Lett.* **85** 4881–3
- [9] Chathoth S M 2011 *Europhys. Lett.* **95** 26001
- [10] Gotze W and Sjogren L 1992 *Rep. Prog. Phys.* **55** 241
- [11] Bernal J D 1960 *Nature* **185** 68–70
- [12] Kuball A, Gross O, Bochtler B and Busch R 2018 *Scr. Mater.* **146** 73–6
- [13] Kuball A, Bochtler B, Gross O, Pacheco V, Stolpe M, Hechler S and Busch R 2018 *Acta Mater.* **158** 13–22
- [14] Wilden J, Yang F, Holland-Moritz D, Szabó S, Lohstroh W, Bochtler B, Busch R and Meyer A 2020 *Appl. Phys. Lett.* **117** 013702
- [15] Basuki S W, Bartsch A, Yang F, Rätzke K, Meyer A and Faupel F 2014 *Phys. Rev. Lett.* **113** 165901
- [16] Basuki S, Yang F, Gill E, Rätzke K, Meyer A and Faupel F 2017 *Phys. Rev. B* **95** 024301
- [17] Griesche A, Macht M-P, Suzuki S, Kraatz K-H and Froberg G 2007 *Scr. Mater.* **57** 477–80
- [18] Bartsch A, Rätzke K, Meyer A and Faupel F 2010 *Phys. Rev. Lett.* **104** 195901
- [19] Zöllmer V, Rätzke K, Faupel F and Meyer A 2003 *Phys. Rev. Lett.* **90** 195502
- [20] Meyer A 2015 The measurement of self-diffusion coefficients in liquid metals with quasielastic neutron scattering *EPJ Web of Conf.* vol 83 (EDP Sciences)
- [21] Günther G and Russina M 2016 *Nucl. Instrum. Methods Phys. Res. A* **828** 250–61
- [22] Russina M and et al 2018 *Physica B* **551** 506–11
- [23] Sears V F 1992 *Neutron News* **3** 26–37
- [24] Lohöfer G and Piller J 2002 The new ISS electromagnetic levitation facility-‘MSL-EML’ *40th AIAA Aerospace Sciences Meeting & Exhibit*
- [25] Egry I, Lohöfer G, Seyhan I, Schneider S and Feuerbacher B 1998 *Appl. Phys. Lett.* **73** 462–3
- [26] Heintzmann P, Yang F, Schneider S, Lohöfer G and Meyer A 2016 *Appl. Phys. Lett.* **108** 241908
- [27] Nell S, Yang F, Evenson Z and Meyer A 2021 *Phys. Rev. B* **103** 064206
- [28] Lamb H 1881 *Proc. London Math. Soc.* **s1–13** 51–70
- [29] Lohöfer G 2018 *Rev. Sci. Instrum.* **89** 124709
- [30] Meyer A 2002 *Phys. Rev. B* **66** 134205

- [31] Yang F, Kordel T, Holland-Moritz D, Unruh T and Meyer A 2011 *J. Phys.: Condens. Matter* **23** 254207
- [32] Yang F, Unruh T and Meyer A 2014 *Europhys. Lett.* **107** 26001
- [33] Boon J and Yip S 1980 *Molecular Hydrodynamics* (New York: McGraw-Hill)
- [34] Meyer A, Busch R and Schober H 1999 *Phys. Rev. Lett.* **83** 5027
- [35] Kuball A 2019 Development, characterization and processing of a novel family of bulk metallic glasses: sulfur-containing bulk metallic glasses *PhD Thesis* Universität des Saarlandes
- [36] Kawamura Y and Inoue A 2000 *Appl. Phys. Lett.* **77** 1114–6
- [37] Pauling L 1947 *J. Am. Chem. Soc.* **69** 542–53
- [38] Einstein A 1926 *Investigations on the Theory of Brownian Motion* ed R furth (New York: Dover)
- [39] Sutherland W 1905 *London Edinburgh Dublin Philos. Mag. J. Sci.* **9** 781–5